Title
Pressure-Induced Phase Transitions of Natural Brookite

Journal
ACS Earth and Space Chemistry, 3(5)

ISSN
2472-3452

Authors
Liu, Weixin
Chen, Jian
Zhang, Xiaoliang
et al.

Publication Date
2019-05-16

DOI
10.1021/acsearthspacechem.8b00213

Peer reviewed

Pressure-Induced Phase Transitions of Natural Brookite

Weixin Liu[1], Jian Chen[1], Xiaoliang Zhang[1], Jinyuan Yan[2], Mingqiang Hou[1,2], Martin Kunz [2], Dongzhou Zhang[3], Hengzhong Zhang[1,*]

[1]Center for High Pressure Science and Technology Advanced Research, Shanghai 201203, China

[2] Advanced Light Source, Lawrence Berkeley National Laboratory, Berkeley, California 94720, USA

[3] Partnership for Extreme Crystallography Program, University of Hawaii at Manoa, Honolulu, Hawaii 96822, USA

KEY WORDS: titania, high pressure, phase transformation, non-hydrostaticity, pressure transmitting medium, shear modulus, equation-of-state, natural mineral

ABSTRACT: The structures and stabilities of the high-pressure phases of titania (TiO_2) are of great interest in the earth sciences, as these phases are the accessible analogs of component minerals in the earth's mantle. Brookite is a natural titania mineral, whose bulk phase is hard to synthesize in the laboratory, and its phase behavior at very high pressure remains unknown. Thus, in this work, using phase-pure natural brookite as the sample, we studied the phase transition of bulk brookite under compression up to ~ 60 GPa in three different pressure transmitting media. Results show that at room temperature and in near hydrostatic conditions, brookite undergoes a series of transitions, i.e., brookite (~ 0 - 12 GPa) → TiO_2-II & minor rutile (~ 1 - 21 GPa) → baddeleyite (~ 12 - 60 GPa) → TiO_2-OI (~ 33 - 60 GPa). Taking into account that all transitions occur at finite rates and that solidification of a pressure medium can influence transition kinetics, we show that the observed transition sequence is consistent with the expected high-

pressure phase stability of TiO_2 calculated from density functional theory. The knowledge obtained from this work may be used to infer the geological fate of brookite in nature.

INTRODUCTION

As a technologically important material, titania (TiO_2) has applications in photocatalysis, gas sensors, energy storage, biotechnology, and cosmetics, etc. Natural titania exists mainly in the three polymorphs, rutile (tetragonal structure), anatase (tetragonal structure) and brookite (orthorhombic structure).[1, 2] Studies show that at ambient pressure, rutile is more stable than anatase at temperatures up to at least ~ 1000 ^{o}C.[3] Anatase and brookite are metastable with respect to rutile and hence, they can transform to rutile upon heating above certain temperatures.[4-7] In nature, brookite often occurs in quartz veins of regional metamorphic rock series or as an accessory mineral in igneous rocks.[8-10] Brookite is relatively rare compared to rutile and anatase.[11] It is very difficult to synthesize bulk brookite in the laboratory, though nanocrystalline brookite can be prepared relatively easily in the lab using different methods.[12-15] Previous high pressure (HP) studies on TiO_2 predominantly focused on the phase transitions of

bulk or nanocrystalline anatase and rutile. Titania phases involved in the subsequent high-pressure phase transitions include columbite (TiO_2-II, space group *Pbcn*), baddeleyite (space group $P2_1/c$), TiO_2-OI (space group *Pbca*), and TiO_2-OII (space group *Pnma*).[16-19] We only found scarce reports on high-pressure behaviors of nanocrystalline brookite at pressures up to ~ 28 GPa[20] and bulk brookite at pressures up to ~ 10 GPa.[11] The phase behavior of bulk brookite at very high pressures (>> 10 GPa) remains unknown possibly because of the unavailability of bulk brookite from laboratory syntheses. However, such knowledge is needed to understand the detailed formation mechanism and stability of brookite. Thus, in this work, using phase-pure natural brookite as the starting material, we studied the pressure-induced phase transitions of natural brookite at room temperature and at pressures up to ~ 60 GPa using *in situ* high-pressure X-ray diffraction (XRD) and Raman spectroscopy. We aim to obtain knowledge about the phase behavior and structural stability of bulk brookite under compression to very high pressures (and in subsequent decompression as well) so that insights into the history and possible fate of natural brookite minerals can be generated with new experimental data.

EXPERIMENTAL SECTION

Sample. The natural brookite sample used in this study was from the mineral collection # 8115 of the Department of Earth and Planetary Science, University of California Berkeley. The mineral was sourced from Magnet Cove, Arkansas, USA. It is similar in appearance to those described in refs. 8 and 9. A few brookite crystals with well-developed morphologies were chosen. The crystals were immersed in a nitric acid solution (1 mol L^{-1}) to dissolve their surface stains and then washed with deionized water before drying and crushing into small pellets. Then, the pellets were ground with a mortar and pestle to very fine powders that were used for the high-pressure study in this work (below).

X-ray Powder Diffraction. To examine the crystal structures of the natural TiO_2 sample, XRD patterns were obtained using an X-ray powder diffractometer (Malvern Panalytical) with Cu K_{α} radiation (wavelength 1.54056 Å). The XRD patterns were collected from 2θ = 10 to 80° at a scanning rate of 5 °/min.

Scanning Electron Microscopy (SEM) and Energy Dispersive Spectroscopy (EDS). The morphologies, particle sizes, and elemental

compositions of the ground titania particles were examined using a scanning electron microscope (VERSA 3D, FEI) equipped with an energy dispersive spectrometer (EDS), which were operated under 5.0 kV/27 pA and 15.0 kV/0.21 nA, respectively.

***In situ* High-Pressure XRD and Raman Spectroscopy**. A diamond anvil cell (DAC) was used to generate the required high pressure of the sample. The culet size of the anvils was 300 μm in diameter. A stainless-steel gasket was pre-indented to 23 μm in thickness, and then a hole of 150 μm in diameter was drilled through the center of the indentation using laser-drilling (at HPSTAR), serving as the sample chamber. A tiny amount of the finely ground brookite powder was compressed into a thin foil at a pressure of ~ 8 MPa using a powder pressing machine. Then, one piece of the thin foil ~ 15 μm thick and an appropriate size for the sample chamber was chosen for loading into the DAC together with a few grains of ruby as the pressure calibrant. A pressure transmitting medium was loaded into the DAC afterwards. Helium, neon and methanol-ethanol mixture (4:1 in volume) were used as the pressure transmitting media for the HP-XRD measurements; a methanol-ethanol mixture (4:1 in volume) was used

as the pressure transmitting medium for the HP-Raman spectroscopy measurements.

In situ HP-XRD measurements were performed at the 12.2.2 beamline station of the Advanced Light Source (ALS) at room temperature.[21, 22] HP-XRD patterns were collected at an X-ray wavelength of 0.4959 Å using a MAR345 image plate detector. The sample-to-detector distance was calibrated using a CeO_2 standard. After compressing the sample near the required pressure value and equilibrating the system for ~ 10 minutes, the sample pressure was measured using laser-fluorescence (excitation laser wavelength 447 nm). Then, the HP-XRD measurement at the given pressure was conducted in the beamline station, taking ~ 5 mins to complete. The HP-XRD and the pressure measurements were repeated at all pressures in the full compression-decompression cycle.

Additional HP-XRD data were collected at the 13-BM-C beamline station of the Advanced Photon Source (APS) at room temperature with an X-ray wavelength of 0.4340 Å. At 13-BM-C. A MAR165 CCD detector was used to collect the diffraction image, and a NIST standard LaB_6 sample was used to calibrate the sample-to-detector distance and the detector tilt. The pressure measurements were similar to those at ALS-

12.2.2 (above) except that the excitation laser had a wavelength of 532 nm. The sample pressure was measured after equilibrating the system for ~ 6 mins and the HP-XRD measurement at each given pressure took ~ 2 mins to complete.

The diffraction images were integrated using the Dioptas program[23] to yield numerical intensity *vs* 2θ data. Rietveld-fitting analyses were performed on the collected XRD patterns using GSAS software[24, 25] to identify and/or verify the phases present, and to obtain the phase contents of the titania phases as a function of pressure.

High-pressure Raman data were collected from 100 to 800 cm^{-1} at room temperature using a Raman spectrometer (inVia Reflex, Renishaw) with a 532 nm excitation laser at ~ 10% of the laser power (83.3 mW). The integration time was 0.029 s for each incremental step of 1 cm^{-1}. At a given pressure, the collection of one Raman spectrum took ~ 20 s.

COMPUTATIONAL SECTION

The enthalpies of the concerned TiO_2 phases (brookite, anatase, rutile, baddeleyite, TiO_2-II, and TiO_2-OI) at different pressures were calculated using density functional theory (DFT) implemented in the Quantum

Espresso (QE) package.[26] The computations were conducted using an integrated graphic user interface and a running environment of QE, Burai (v.1.3.2).[27] The projector augmented-wave (PAW) pseudopotential functions[28] of Ti and O with an energy cutoff of ~ 52 Ry and charge density cutoff of ~ 575 Ry, and PBE exchange-correlations[29] at the GGA+U approximation[30] were used for the calculations, where the Hubbard correction parameter U was taken as 5.0 eV for both the Ti and O atoms.[31] At a given pressure, the crystal structure of a Ti-O phase was optimized and the enthalpy of the phase was obtained. The enthalpy relative to rutile at the same pressure could then be calculated and used to determine the relative phase stability of various titania phases at different pressures.

The enthalpy of a high-pressure titania phase (baddeleyite or TiO_2-OI) was also calculated under compression with unequal pressures acting on different crystallographic orientations of the crystal (see Figure S1 & Table S1, Supporting Information (SI)). First, the crystal was hydrostatically compressed in all orientations at a pressure P, generating a geometrically optimized structure and enthalpy. Then, the crystal was non-hydrostatically compressed under an axial pressure of $P_{ax} = P + 5$ (GPa) and two perpendicular radial pressures of

$P_{rad} = P$ under the constraint that only the axial dimension was free to change. This produced another geometrically optimized structure and enthalpy. The enthalpy of the non-hydrostatic case (at $P_{ax} = P + 5$ (GPa) and $P_{rad} = P$) relative to that of the hydrostatic case (at $P_{ax} = P + 5$ (GPa)) reflects the effect of the non-hydrostaticity on the enthalpy of the high-pressure phase.

RESULTS AND DISCUSSION

Sample Characterization. A photo of the natural brookite crystals is shown in Figure 1a. The single crystals are black in color and have pseudohexagonal bipyramid shapes with sizes ranging from ~ 2.2 to 4.5 mm. One of the crystals is twinned with another smaller one.

The XRD pattern at ambient pressure of the brookite sample is shown in Figure 1b. Rietveld analysis confirmed that the sample is a single-phase brookite (ICSD #15409[32]), since all the diffraction peaks can be indexed as reflections from the brookite structure in the *Pbca* space group.[33] The XRD pattern of the brookite thin foil for loading into the DAC is almost identical to that of the powder sample before pressing (Figure S2). This indicates that no phase transition had

occurred in the pre-processing of the brookite sample before applying GPa-scale pressures in the DAC.

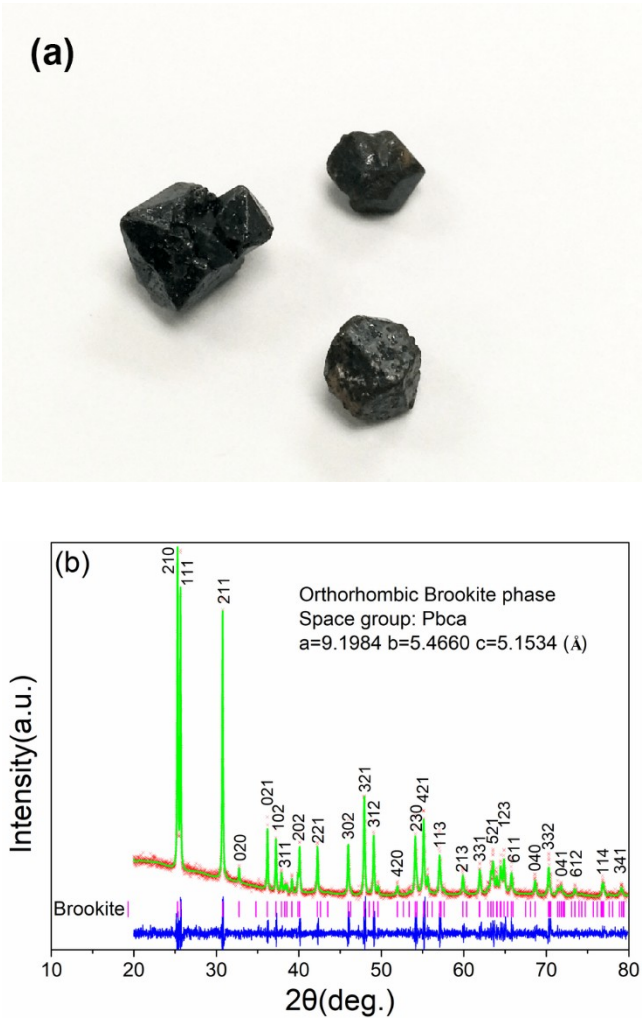

Figure 1. (a) Photo of natural brookite crystals; (b) Rietveld fitting of the X-ray diffraction pattern of natural brookite at ambient pressure.

Figure 2a shows the SEM image of the ground fine brookite particles. Two locations of a particle were chosen for elemental analysis using EDS (Figure 2b); the corresponding EDS spectra are shown in Figures 2c & 2d. EDS results (Table 1) show that the natural brookite sample consists of TiO_2 (atomic ratio of Ti:O ≈ 1:2) with trace amount of niobium that causes the black color of the natural brookite crystals.[8, 10]

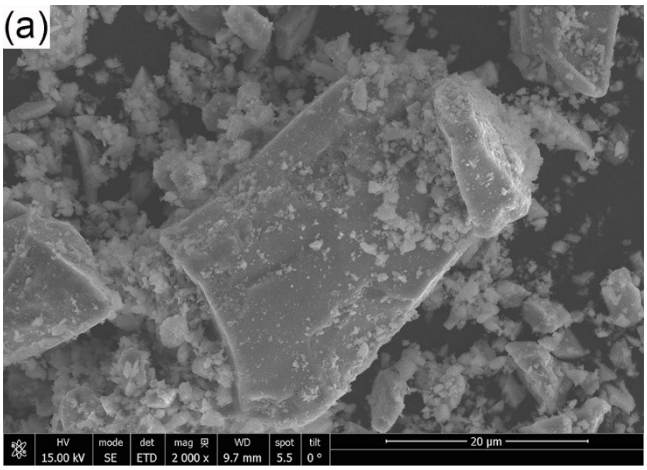

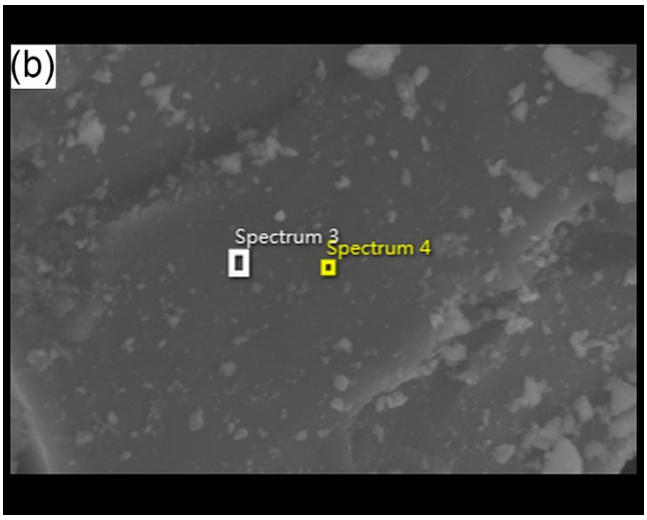
(b)
Spectrum 3
Spectrum 4

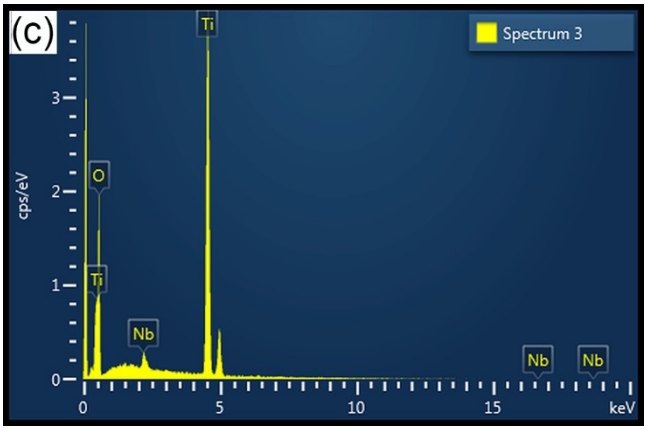
(c)
Spectrum 3
Ti
O
Ti
Nb
Nb
Nb
cps/eV
0
1
2
3
0
5
10
15
keV

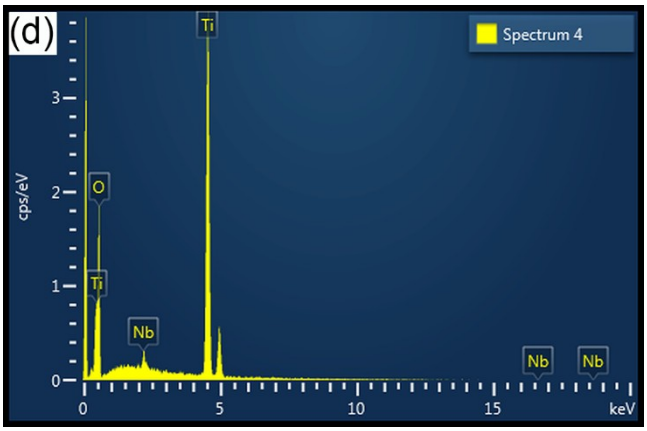
(d)
Spectrum 4
Ti
O
Ti
Nb
Nb
Nb
cps/eV
0
1
2
3
0
5
10
15
keV

Figure 2. SEM image of the natural brookite particles produced from crushing and grinding a brookite crystal (a), chosen sample locations for the EDS analyses (b), and the EDS spectra from the chosen locations (c, d).

Table 1. Major Chemical Composition of the Natural Brookite Sample

Element	Average weight percent (%)	Average atomic percent (%)
O	38.64	65.72
Ti	59.23	33.65
Nb	2.13	0.63
Total:	100	100

***In Situ* High Pressure XRD.** Figure 3 shows the HP-XRD patterns of natural brookite under compression using three different kinds of pressure (P) transmitting media: helium (Figure 3a), neon (Figures 3b & 3c), and a methanol-ethanol mixture (Figures 3d & 3e) at pressures up to ~ 60 GPa. According to ref. 34, He, Ne, and the methanol-ethanol mixture solidify at 12.1, 4.8 GPa and 10.5 GPa at room temperature, respectively. Before their solidification, they are all hydrostatic, i.e., the deviatoric stress across a sample is ~ 0 GPa. Even after solidification,

in a gasket bore of 80 to 200 μm, the deviatoric stress is < 0.15 GPa at 40 GPa in He and < 0.5 GPa at 50 GPa in Ne,[34] which make them quasi-hydrostatic in a wide range of pressures. However, in the methanol-ethanol mixture, the deviatoric stress increases dramatically with pressure, e.g., it is ~ 2.5 GPa at ~ 22 GPa.[34] Thus, the non-hydrostaticity of the three pressure media increases in the order of helium, neon, and methanol-ethanol mixture. Using the three P media allows us to investigate the influences of their hydrostaticity and elastic properties on the phase transition of natural bulk brookite.

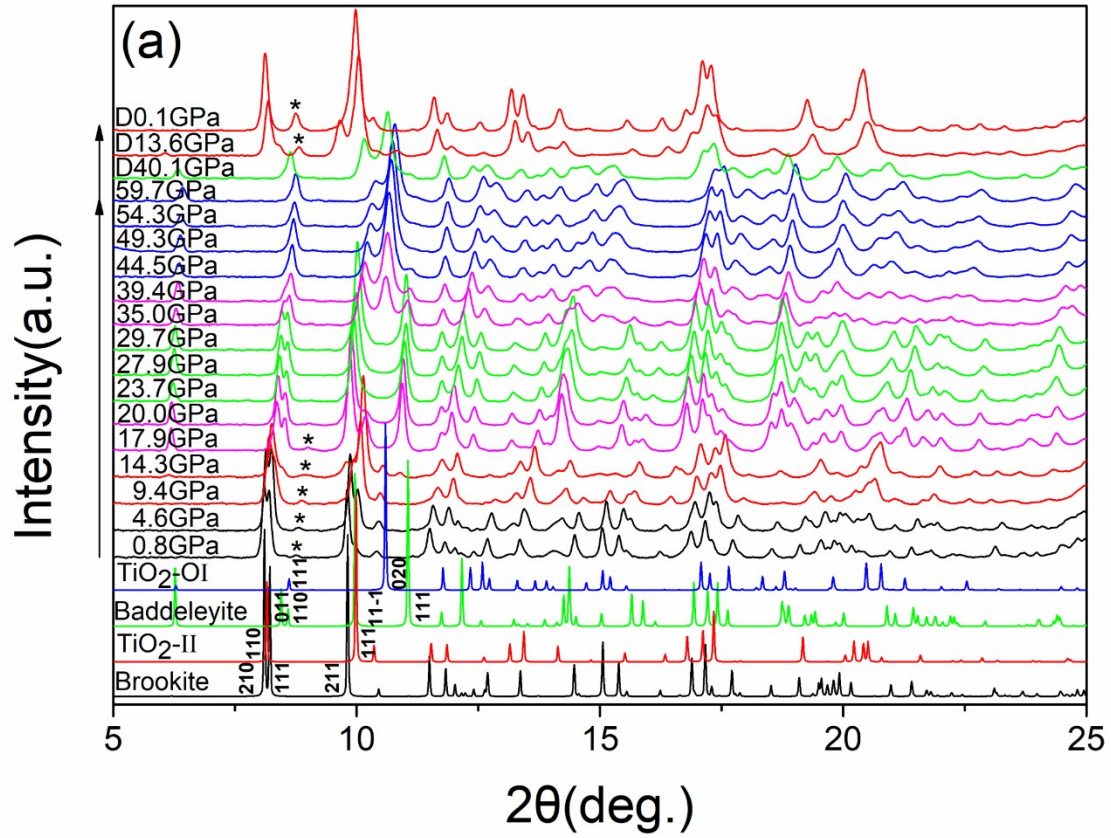
(a)
D0.1GPa
D13.6GPa
D40.1GPa
59.7GPa
54.3GPa
49.3GPa
44.5GPa
39.4GPa
35.0GPa
29.7GPa
27.9GPa
23.7GPa
20.0GPa
17.9GPa
14.3GPa
9.4GPa
4.6GPa
0.8GPa
TiO2-OI
Baddeleyite
TiO2-II
Brookite
Intensity(a.u.)
2θ(deg.)
5
10
15
20
25

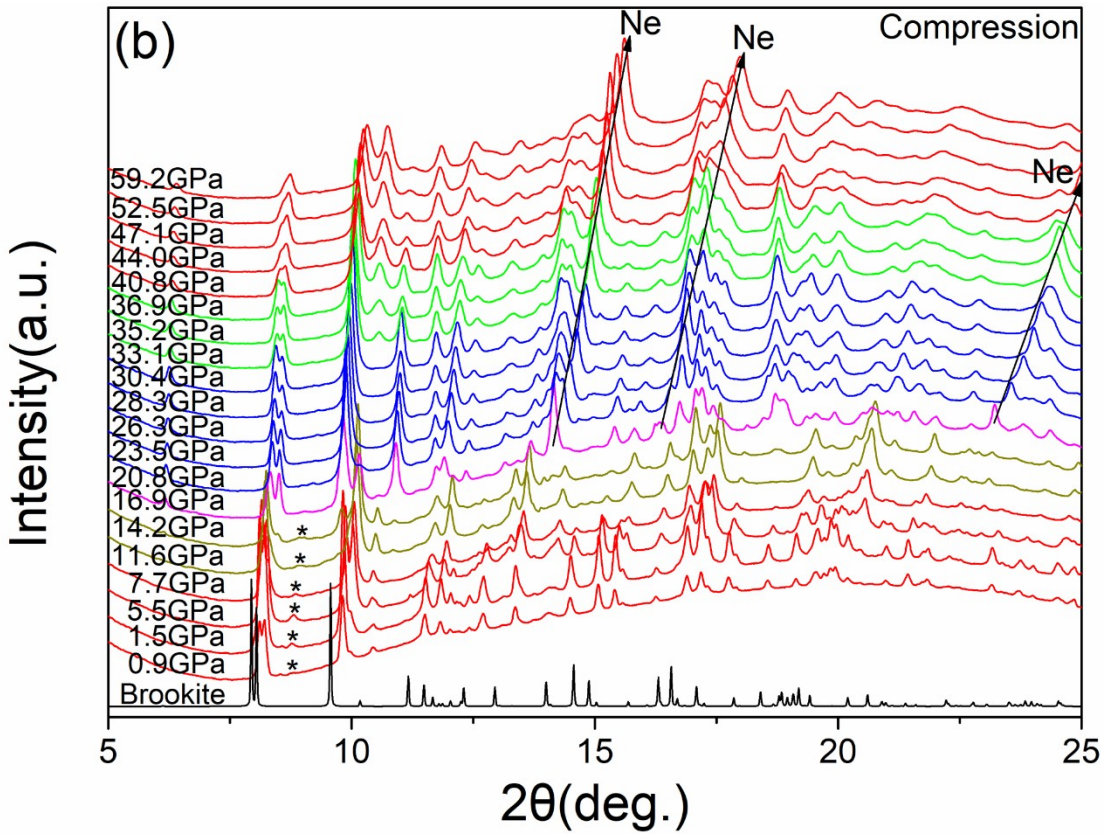
(b)
Ne
Ne
Ne
Compression
59.2GPa
52.5GPa
47.1GPa
44.0GPa
40.8GPa
36.9GPa
35.2GPa
33.1GPa
30.4GPa
28.3GPa
26.3GPa
23.5GPa
20.8GPa
16.9GPa
14.2GPa
11.6GPa
7.7GPa
5.5GPa
1.5GPa
0.9GPa
Brookite
*
Intensity(a.u.)
5
10
15
20
25
2θ(deg.)

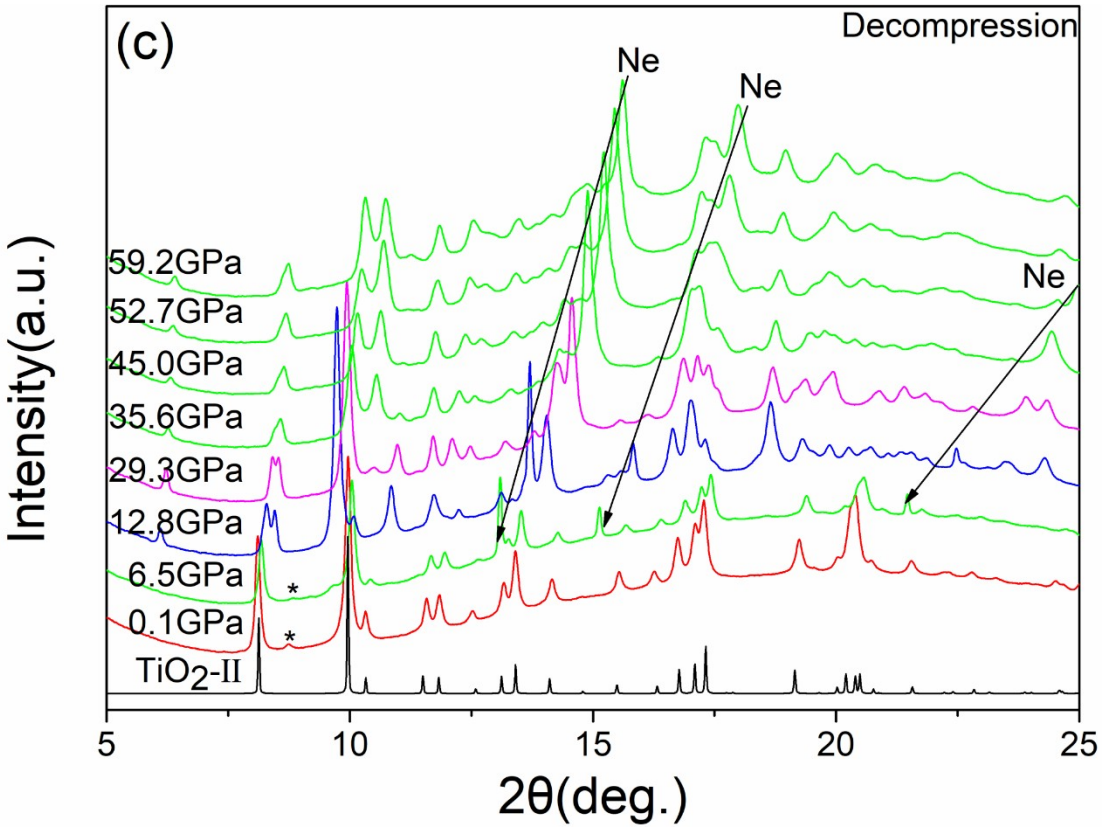
(c)
Decompression
Ne
Ne
Ne
59.2GPa
52.7GPa
45.0GPa
35.6GPa
29.3GPa
12.8GPa
6.5GPa
0.1GPa
TiO2-II
*
*
Intensity(a.u.)
5
10
15
20
25
2θ(deg.)

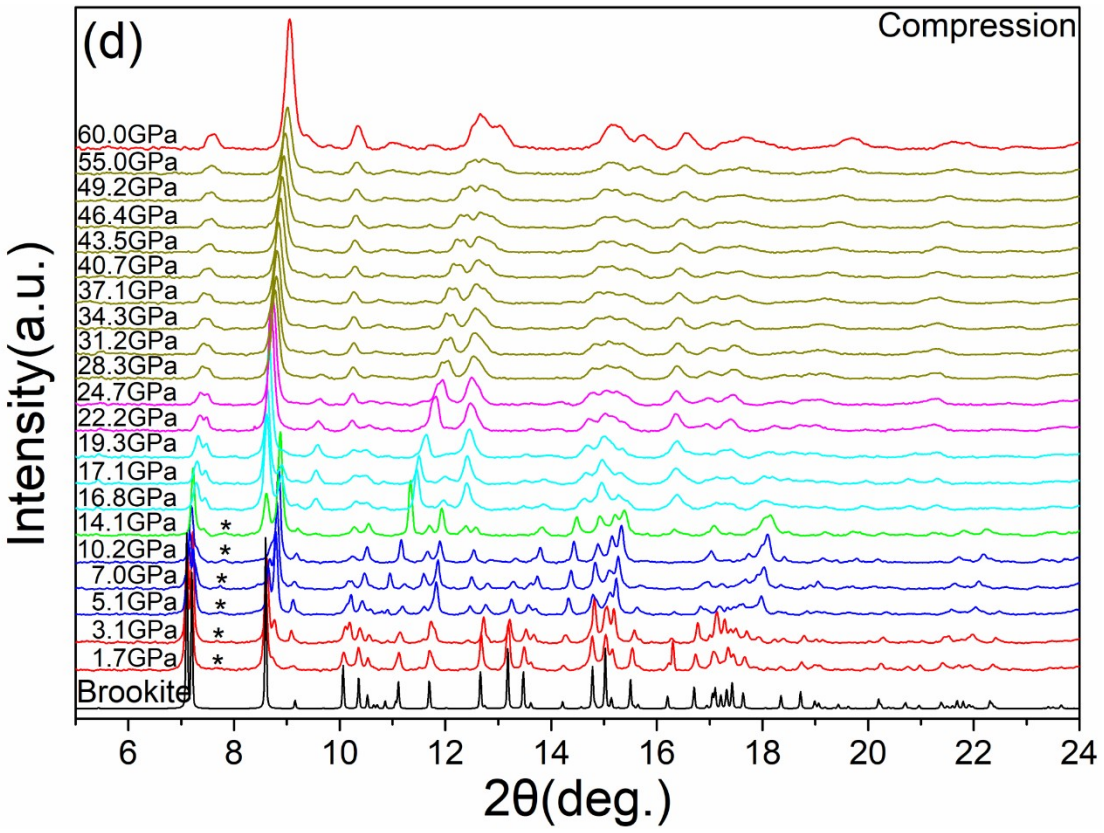
(d)
Compression
60.0GPa
55.0GPa
49.2GPa
46.4GPa
43.5GPa
40.7GPa
37.1GPa
34.3GPa
31.2GPa
28.3GPa
24.7GPa
22.2GPa
19.3GPa
17.1GPa
16.8GPa
14.1GPa
10.2GPa
7.0GPa
5.1GPa
3.1GPa
1.7GPa
Brookite
*
Intensity(a.u.)
6
8
10
12
14
16
18
20
22
24
2θ(deg.)

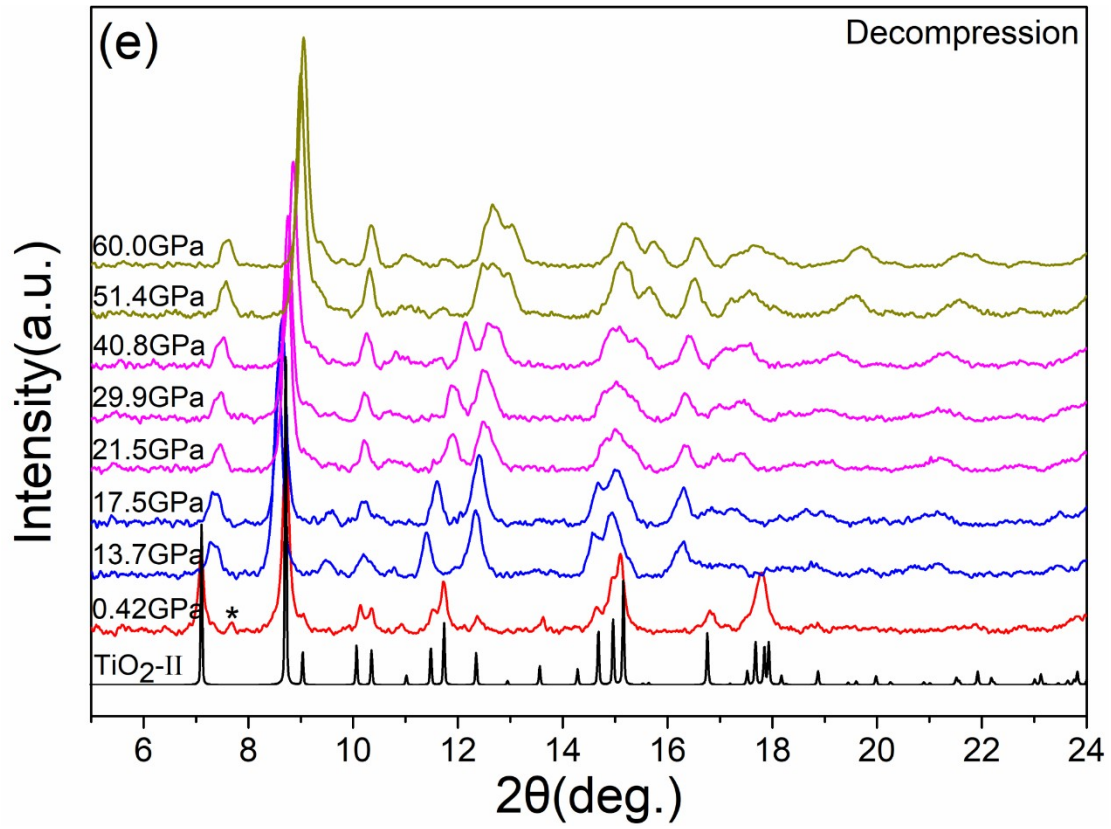

Figure 3. High-pressure XRD patterns of natural brookite under compression using pressure transmitting media of helium (a), neon (b & c), and methanol-ethanol (4:1 in volume) (d & e). Data in (a - c) were collected at ALS-12.2.2 beamline station and those in (d & e) at the APS-13-BMC beamline station. In (a), prefix “D” in the pressure values indicates decompression. The calculated XRD patterns under ambient pressure are shown at the very bottom of each diagram for reference. Star symbols (*) denote rutile (110) peaks.

The XRD patterns of the bulk brookite under compression in helium are shown in Figure 3a. A series of phase transitions occurred during compression of the sample. By comparing these with the calculated XRD patterns of reference TiO_2 phases (bottom of Figure 3a) and using Rietveld analyses (representative fittings are shown in Figure 4), the present phases were identified. Rietveld analyses show that small amounts of TiO_2-II phase (space group *Pbcn,* ICSD #15328[32]) and rutile (space group $P4_2/mnm$, ICSD #9161[32]) appeared at pressures as low as 0.8 GPa (Figure 4a),. At 9.4 GPa, the majority of brookite had transformed to TiO_2-II and minor rutile. At 14.3 GPa, brookite disappeared. Meanwhile, the formed TiO_2-II and the minor rutile started to transform to baddeleyite (space group $P2_1/c$, COD # 9015355[35]) and the transformations completed at ~ 23.7 GPa (Figure 3a). The baddeleyite phase remained a single phase between 23.7 and 29.7 GPa, above which it started to transform to and coexist with TiO_2-OI (space group *Pbca*[18]) up to the maximum experimental pressure (59.7 GPa) (Figure 3a). The coexistence of the two phases in such a wide pressure range (~ 35 – 60 GPa; Figure 3a) may be attributed to the similarity between the two structures.[36-39] During decompression, TiO_2-OI converted back to baddeleyite (Figure 3a). When decompressed to

13.6 GPa, TiO_2-OI disappeared while TiO_2-II and small amounts of rutile reappeared, coexisting with baddeleyite. Upon full decompression to ~ 0.1 GPa, baddeleyite converted almost fully to TiO_2-II coexisting with a small amount of rutile (Figure 3a). From the Rietveld analyses of all the XRD patterns in Figure 3a, the variations of the phase contents of various titania phases with pressure are depicted in Figure 5a. This diagram shows clearly the phase behavior of bulk brookite under compression in a helium medium.

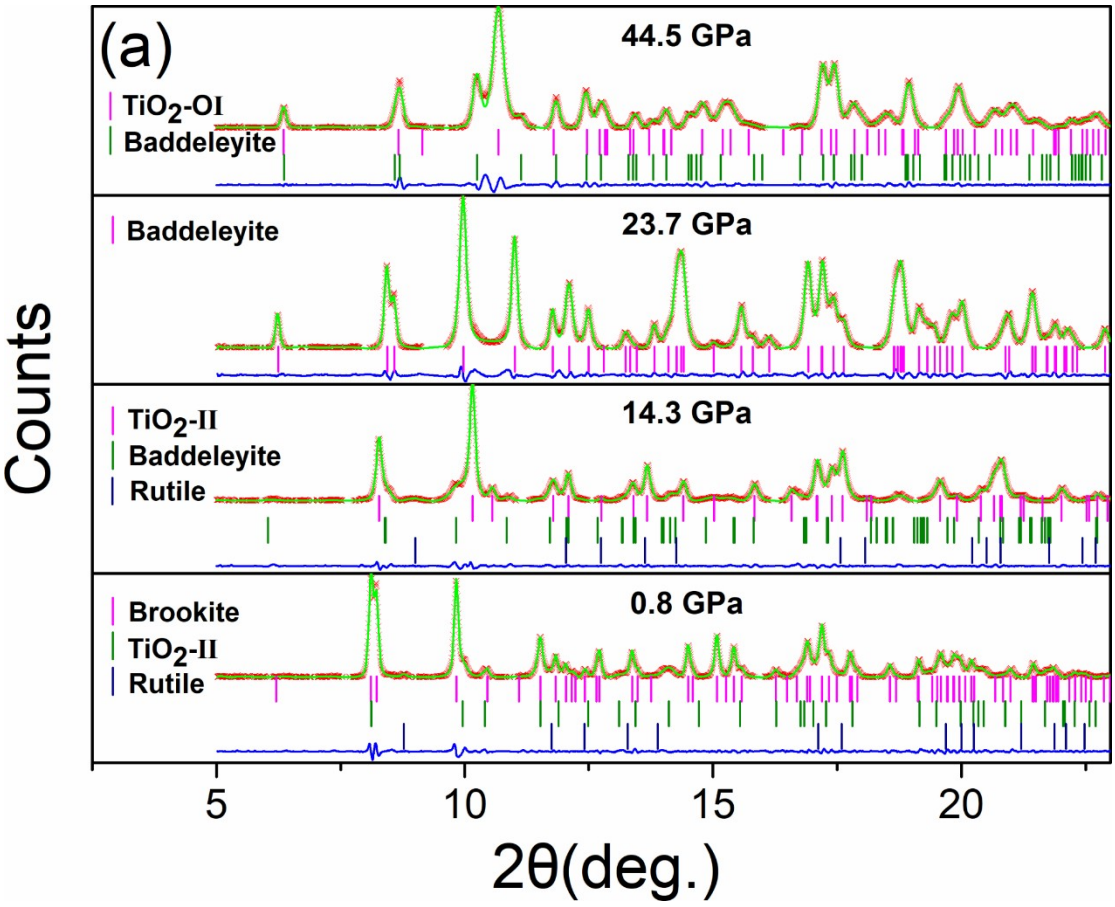

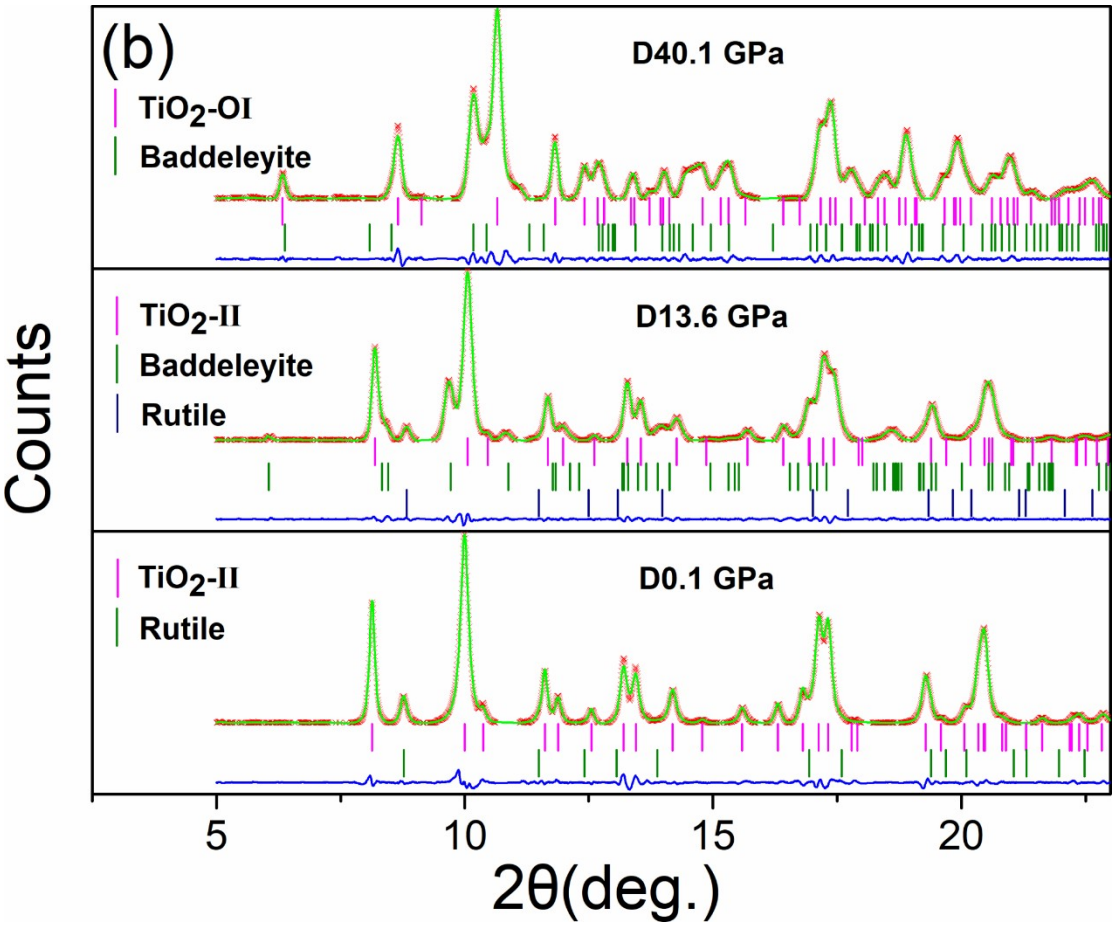

Figure 4. Representative Rietveld fitting of XRD patterns (shown in Figure 3a) of natural brookite during compression (a) and decompression (b). The derived lattice parameters and phase contents are listed in Table S2.

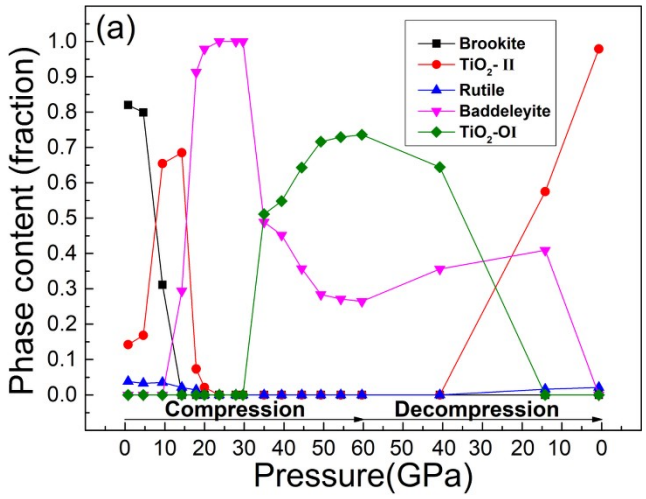
(a)
Brookite
TiO2- II
Rutile
Baddeleyite
TiO2-OI
Phase content (fraction)
Compression
Decompression
Pressure(GPa)

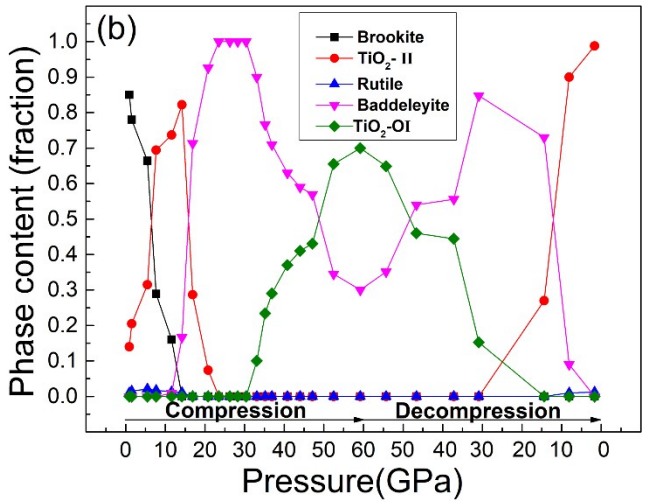
(b)
Brookite
TiO2- II
Rutile
Baddeleyite
TiO2-OI
Phase content (fraction)
Compression
Decompression
Pressure(GPa)

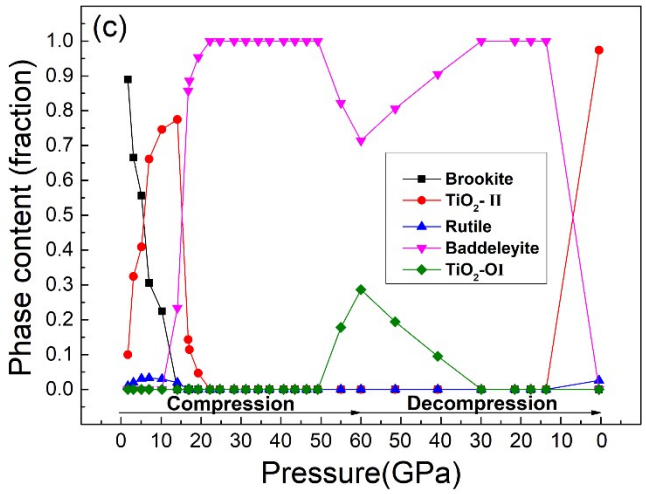

Figure 5. The pressure dependence of phase contents of TiO_2 phases occurring during the compression and decompression of the natural brookite sample using pressure transmitting media of helium (a), neon (b), and methanol-ethanol (4:1 in volume) (c).

Similarly, the phases present during compression and decompression in the neon pressure medium (Figures 3b & 3c) or methanol-ethanol mixture (Figures 3d & 3e) were identified using the same methods as the one used for Figure 3a. The variations of the phase contents with pressure in these two media are illustrated in Figure 5b and Figure 5c, respectively. The three diagrams in Figure 5 show that the phase behaviors of bulk brookite in both helium and

neon are similar at all P, indicating that their (quasi-) hydrostaticity are nearly equal and affect the phase behavior of brookite in the same way. Phase transitions of bulk brookite in the methanol-ethanol mixture (Figure 5c) are also similar to those in helium (Figure 5a) and neon (Figure 5b) in the hydrostatic pressure range (< ~ 11 GPa[34]). However, they deviate from those in the latter two media significantly at > ~ 11 GPa: in methanol-ethanol, the baddeleyite phase fully formed from brookite at ~ 25 GPa could remain up to ~ 50 GPa before transforming to TiO_2-OI (Figure 5c), while in helium and neon, the baddeleyite also fully formed at ~ 25 GPa but started to transform to TiO_2-OI as low as ~ 30 GPa (Figures 5a & 5b). Moreover, during decompression, baddeleyite could also retain its single phase between ~ 30 and ~ 15 GPa in the methanol-ethanol medium (Figure 5c), while in helium and neon, no single baddeleyite phase was observed (Figures 5a & 5b). These differences demonstrate that the hydrostaticity and the related elasticity of a pressure medium can modify the phase behavior of titania markedly: non-hydrostaticity favors stabilization of the baddeleyite phase as a single phase. This phenomenon may be interpreted as a result of the solidification of the methanol-ethanol mixture, as the solidified glassy and stiff mixture can introduce lattice

strains in the titania phases, impacting the transition kinetics. Because baddeleyite has a lower symmetry (monoclinic) than the other occurring phases (either orthorhombic or tetragonal), it can accommodate more lattice strains (due to less geometric constraint on the unit cell) than them (due to more geometric constraints on the unit cells). Thus, non-hydrostaticity (and related medium properties) tends to slow down or even inhibit the transition from baddeleyite to TiO_2-OI.

Figure 5 should be treated as non-equilibrium (i.e., kinetic) state diagrams as they deal with the behavior of a metastable phase (brookite), show the path dependent behavior (e.g., difference between compression and decompression), and do not conform to the equilibrium phase rule. If the TiO_2 system were to be in equilibrium at room temperature under compression, the maximum number of coexisting phases is $P = C + 1 - F = 1 + 1 - 0 = 2$. However, in our experiments, three phases occurred concurrently at some pressures (e.g., at 9.4 GPa in compression in Figures 5a). This happened because non-hydrostatic stress provides an additional degree of freedom at some of the experimental conditions, allowing the occurrence of competing phase transitions from one phase (or two phases) to the

other two phases (or another phase). For instance, at 9.4 GPa in compression, brookite → TiO_2-II and brookite → rutile (Figures 3a & 5a).

High-Pressure Raman Spectroscopy. High pressure Raman measurements of the natural bulk brookite (Figure 6) were conducted to confirm the phase transitions observed by XRD (Figures 3d & 3e). As shown in Figure 6a, the Raman peaks observed at 1.1 GPa are in good agreement with the predicted vibrational bands of brookite[40]: A_{1g} (127, 155, 192, 246, 414, 643 cm^{-1}), B_{1g} (136, 155, 213, 322, 414, 504 cm^{-1}), B_{2g} (366, 464, 586 cm^{-1}), and B_{3g} (172, 286, 547, 449 cm^{-1}),[40, 41] among which the band at 155 cm^{-1} is the strongest. Upon further compression to 5.8 GPa, the Raman bands of the TiO_2-II phase[42-44] became obvious, while the Raman bands of brookite became weak and almost disappeared at 11.1 GPa. When the pressure reached 19.8 GPa, all TiO_2-II Raman peaks disappeared, while the baddeleyite Raman peaks[42-44] appeared and then became significantly broader and weaker under further compression to 45.0 GPa. From 49.3 to 59.6 GPa, a sharp Raman peak at ~ 295 cm^{-1} appeared, indicating the TiO_2-OI phase, and hence, the Raman spectra consisted of contributions from both the baddeleyite and TiO_2-OI phases.

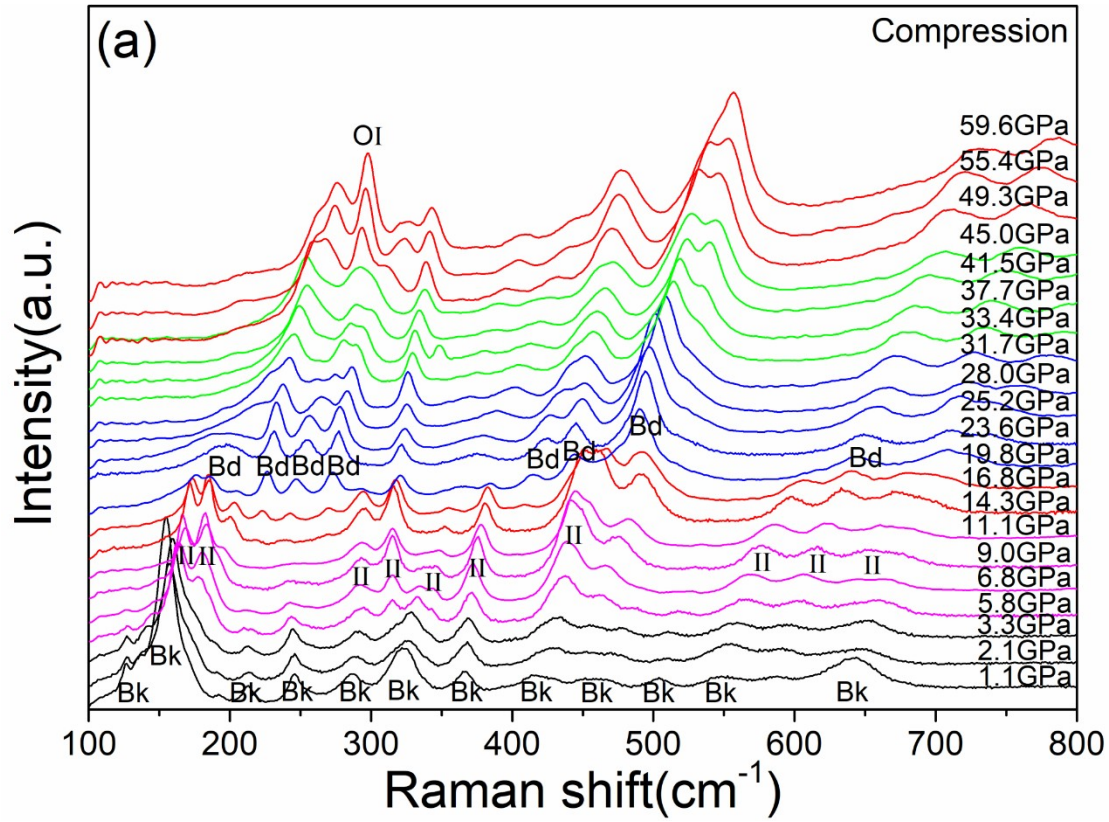
(a)
Compression
OI
59.6GPa
55.4GPa
49.3GPa
45.0GPa
41.5GPa
37.7GPa
33.4GPa
31.7GPa
28.0GPa
25.2GPa
23.6GPa
19.8GPa
16.8GPa
14.3GPa
11.1GPa
9.0GPa
6.8GPa
5.8GPa
3.3GPa
2.1GPa
1.1GPa
Bd
II
Bk
Intensity(a.u.)
100
200
300
400
500
600
700
800
Raman shift(cm-1)

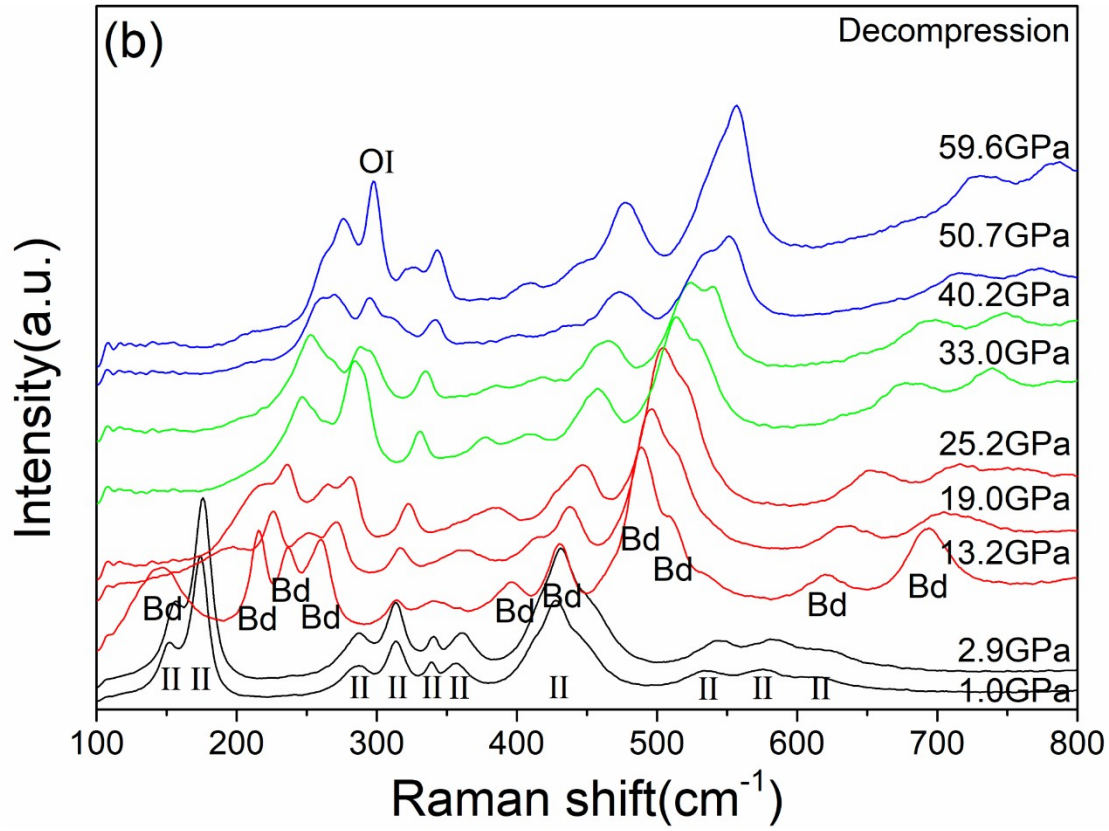
(b)
Decompression
OI
59.6GPa
50.7GPa
40.2GPa
33.0GPa
25.2GPa
19.0GPa
13.2GPa
2.9GPa
1.0GPa
Bd
II
Intensity(a.u.)
100
200
300
400
500
600
700
800
Raman shift(cm-1)

Figure 6. High-pressure Raman spectra of natural brookite under compression (a) and decompression (b) using a methanol-ethanol mixture (4:1 in volume) as the pressure transmitting medium. “Bk”, “Bd”, “OI”, and “II” denote brookite, baddeleyite, TiO_2-O59I, and TiO_2-II (α-PbO_2) phases, respectively.

During decompression from 59.6 to 33.0 GPa (Figure 6b), the TiO_2-OI Raman peaks became progressively weaker while those of baddeleyite became stronger. On further decompression to 13.2 GPa, the Raman spectra were dominated by baddeleyite. When the pressure decreased to 2.9 GPa, the TiO_2-II Raman bands increased significantly, which were retained at 1.0 GPa. Rutile Raman bands were not observed in decompression to near the ambient pressure, as would be expected from the XRD data (Figure 5c). We interpret this is due to the very low content of rutile. Overall, the high-pressure Raman spectroscopy data of the phase transitions of natural brookite in a methanol-ethanol P medium are in good agreement with the XRD results (Figure 5c).

In the Raman measurements, laser illumination on a sample might produce heat, causing thermally-activated phase transitions in brookite. However, as the applied laser power was low and the exposure time was short (see above), any heat generated could be easily dissipated into the gasket via the pressure medium and then to the DAC set. In addition, the thermally-activated brookite-to-rutile transition requires very high temperature (over 800 ^{o}C).[45] This temperature is unlikely to have been achieved by the Raman laser illumination in our experiments. Thus, the phase transitions observed in the HP-Raman measurements can all be attributed to the pressure effects.

Sequences of Phase Transitions of Bulk Brookite under Compression. Our experimental results (Figure 5) show that under compression, bulk brookite follows the phase transition sequence of brookite → TiO_2-II (+minor rutile) → baddeleyite → TiO_2-OI, whereas during decompression it is TiO_2-OI → baddeleyite → TiO_2-II (+minor rutile). In comparison, nano brookite transforms to baddeleyite directly.[20] Such a difference may be related to the increased free energy of nanoparticles, which is size- and morphology-dependent,

causing modified phase behavior and transition sequence in nanoparticles.[46]

Previous experimental and theorical works show that under compression, bulk anatase or rutile follows the phase transition sequence of anatase/rutile → TiO_2-II → baddeleyite → TiO_2-OI → TiO_2-OII.[18, 19, 47-49] In this respect, the pressure-induced phase transitions of bulk brookite resemble those of bulk anatase and bulk rutile. However, the observed temperatures for the TiO_2-OI phase formation are quite different, as discussed below.

Theoretical calculations predicted the presence of TiO_2-OI in the pressure range of ~ 45 – 70 GPa (300 K),[18] above ~ 40 GPa (0 K),[18] or in ~ 20 – 40 GPa (0 K).[50] Experimentally, TiO_2-OI occurred at 1300 – 1500 K by laser heating and in the pressure range of 28 – 32 GPa.[18] In another experiment, TiO_2-OI was observed at 2200 – 2500 K in laser heating and in the pressure range of 35.3 – 36.2 GPa.[51] In contrast to these, TiO_2-OI formed at room temperature at ~ 33 GPa in helium/neon media (Figures 5a & 5b) or ~ 50 GPa in methanol-ethanol medium (Figure 5c) in our experiments using bulk brookite as the starting material. Moreover, the formed TiO_2-OI was stable at P up to the maximum experimental pressure of ~ 60 GPa. The formation pressure

of bulk TiO_2-OI in quasi-hydrostatic conditions (~ 33 GPa) is far less than the predicted pressure of 45 – 70 GPa.[18] Yet, it is close to the experimentally observed pressures in the laser heating experiments of ~ 28 – 32 GPa[18] or ~ 35 – 36 GPa.[51] These indicate that using brookite as the starting material can alter the phase transition kinetic route so that the kinetic barrier can be reduced significantly.

Figure 5 reveals that in the methanol-ethanol medium at high pressure, the non-hydrostaticity and the change in the medium elasticity (see below) can inhibit the baddeleyite → TiO_2-OI transition (Figure 5c vs. Figures 5a & 5b), making the transition pressure (~ 50 GPa) much higher than those in more hydrostatic conditions (~ 33 GPa). In previous laser heating experiments, no pressure medium[18] or NaCl medium[51] was used, which would produce less or no hydrostatic conditions. Again, this would introduce high lattice strain in baddeleyite, stabilizing baddeleyite at high pressures (see above). Consequently, much higher temperatures (> 1000 ºC) were needed to trigger the baddeleyite → TiO_2-OI transition with laser heating in these works.[18, 51]

Understanding the Phase Transition Sequences of Brookite using Computations. The phase stabilities at both ambient and high

pressures of various titania phases have been studied extensively using different kinds of computational methods,[31, 50, 52-56] achieving different levels of success in terms of consistency with the available experimental data. It was proven that it is non-trivial to correctly model the phase stability of the titania system as a function of either or both of the temperature and pressure.[31] For example, to correctly reproduce the observed high-pressure phase transitions among anatase, rutile, and TiO_2-II using the DFT+U method, the Hubbard parameter U should equal 5 eV.[31] Based on this, we chose U = 5 eV in our computations using the DFT+U method. Figure 7 shows our calculated enthalpies of the concerned titania phases at different pressures. Using the calculated lattice parameters and hence, the unit cell volumes as a function of pressure, we also derived the bulk moduli of several TiO_2 phases by fitting the data to the equations-of-state (EOS) (see Figure S3). Results in Table S3 show that the DFT-derived bulk moduli agree fairly well with those derived from the experimental data (Figure S4). By contrast, the bulk moduli from a previous DFT work[57] without the Hubbard correction deviate appreciably from the experimental results (except for TiO_2-II).

Our DFT calculation results show that, at ambient temperature and pressure, ΔH(rutile → anatase) = 3.0 kJ mol^{-1} and ΔH(rutile → brookite) = 5.5 kJ mol^{-1} (Figure 7). Using the experimentally determined entropies of rutile (50.4 J mol^{-1} K^{-1}),[3] anatase (49.8 J mol^{-1} K^{-1})[3], and brookite (52.6 J mol^{-1} K^{-1}),[58] the entropy contribution to the free energy change is $-T\Delta S$(rutile → anatase) = 0.2 kJ mol^{-1} and $-T\Delta S$(rutile → brookite) = -0.7 kJ mol^{-1}, accounting for 6.2% and 14.6% of the total free energy change (i.e., $|T\Delta S/(\Delta H - T\Delta S)|$), respectively. As the pressure increases, the entropy contribution ($|T\Delta S/(\Delta U + P\Delta V - T\Delta S)|$) decreases. Based on this, and considering that experimental entropies of other involving phases are unavailable, we used the enthalpies of the TiO_2 phases to analyze the phase transitions of TiO_2.

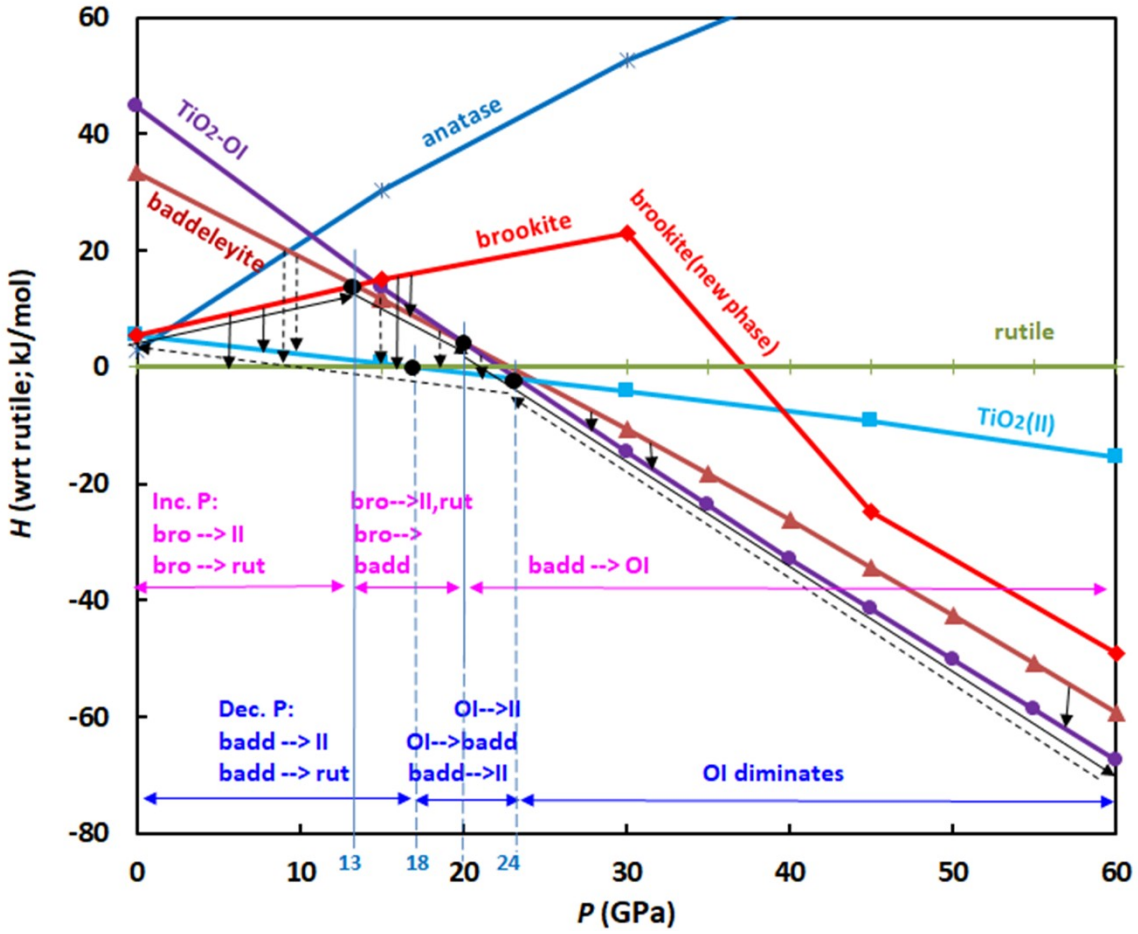

Figure 7. Calculated enthalpies of titania phases relative to that of rutile as a function of pressure. The downward solid (dashed) arrow indicates a possible phase transition from a high-enthalpy phase to a low-enthalpy phase during compression (decompression); the slanted solid and dashed arrows denote the enthalpy routes in compression and decompression, respectively; the solid (dashed) vertical line indicates the energy crossover between the two phases during

compression (decompression). The drastic slope change of the enthalpy curve of brookite at 30 GPa is due to its spontaneous change to a new structure (phase) in the DFT geometric optimization.

Figure 7 shows possible phase transitions following the enthalpy routes during brookite compression and decompression, taking into account the transition kinetics (i.e., a transition only proceeds at a limited rate rather than instantaneously). During compression at P below 13 GPa, brookite is metastable with respect to rutile and TiO_2-II. Thus, brookite can transform to rutile and TiO_2-II via competing reactions. This is consistent with the experimental data (Figures 3 & 5) that shows the formation of TiO_2-II and rutile from brookite. The experimentally formed rutile has a lower content than TiO_2-II, while in Figure 7 at P < 18 GPa, rutile has a lower enthalpy and hence, it should be more stable and have a higher content than TiO_2-II. If the entropies of the involved phases[52, 58] are considered, ΔG(brookite → rutile) = -5.5 - 0.3×(51.4 – 52.6) = -5.1 kJ mol^{-1} and ΔG(brookite → TiO_2-II) = (5.4 – 5.5) – 0.3×(48.4 – 52.6) = 1.16 kJ mol^{-1} at ambient pressure. This means that around ambient pressure, the transition from brookite to rutile is even more thermodynamically favorable than brookite to TiO_2-

II. Thus, the difference between the theoretical expectation and the experimental data suggests that there is a faster transition kinetics from brookite to TiO_2-II than to rutile due to the similarity between the TiO_2-II and brookite structures, as they differ only in the stacking arrangement of similar structural layers.[4, 59] On compression between 13 and 20 GPa, unreacted brookite continues to transform to TiO_2-II and rutile, and to baddeleyite, as the enthalpy of the latter now becomes lower than that of brookite (Figure 7). This also agrees with the experimental data in Figure 5, though experimentally the contents of rutile and TiO_2-II diminish with the increase of P. The fast increase of the baddeleyite content above ~ 15 GPa (Figure 5) suggests that there is a faster transition kinetics from brookite to baddeleyite than to TiO_2-II and rutile.

Upon further compression above 20 GPa up to the maximum P of 60 GPa, TiO_2-OI phase has a lower enthalpy than baddeleyite (Figure 7). Thus, the previously formed baddeleyite should transform to the TiO_2-OI phase. However, experimentally, this transition was not observed until P above ~ 30 GPa (Figures 5a & 5b) or ~ 50 GPa (Figure 5c). Such a hysteresis is related to the shear modulus of the pressure medium.[60] The onset transition pressure deviates more from the

equilibrium value in a pressure medium with a lower shear modulus (G).[60] According to ref. [61], under compression, the shear modulus of helium has a magnitude that is almost the same as that of the pressure itself (e.g., at P = 30 & 50 GPa, $G \approx$ 30 & 50 GPa). Using the bulk modulus data of methanol measured by Zaug et al.,[62] we estimated that the shear modulus of methanol is $G \approx$ 14 & 22 GPa at P = 30 & 50 GPa, respectively (see SI). If the elastic behaviors of helium and neon are similar and those of methanol and ethanol are similar, then we would expect the onset pressure of the baddeleyite → TiO_2-OI transition in the helium/neon medium to be lower than that in the methanol-ethanol mixture. This deduction is consistent with the experimental results shown in Figures 5.

It is also possible that the non-hydrostaticity of a pressure medium (after its solidification) may also contribute to the hysteresis in the baddeleyite → TiO_2-OI transition. Results from our DFT calculations show that the non-hydrostaticity can indeed delay the transition, making baddeleyite more stable by ~ 0.1 – 0.2 kJ/mol than at hydrostatic conditions (see Table S1). However, this effect is minor compared to the effect of shear modulus of a pressure medium (above).

Similar analyses can also be applied to the decompression process, which also shows a good agreement between the predicted phase transition sequences (Figure 7) with the experimental ones (Figures 5a & 5b). Experimentally, metastable TiO_2-II dominated during decompression below ~15 GPa possibly because of the higher transition kinetics from baddeleyite to TiO_2-II than to rutile.

The above analyses show that the calculated relative enthalpy diagram of TiO_2 is consistent with observations when additional degrees of freedom (from non-hydrostatic pressure) and their influence on kinetics are considered in conjunction.

CONCLUSIONS

At room temperature and under compression up to ~ 60 GPa, natural brookite undergoes a series of phase transitions at attainable kinetics, driven by a decrease in the free energy. Below ~ 21 GPa, brookite exhibits similar transition behaviors in three kinds of pressure media, helium, neon, and methanol-ethanol mixture: brookite (~ 0 - 12 GPa) → TiO_2-II & minor rutile (~ 1 - 21 GPa) → baddeleyite (~ 12 – 21 GPa). A single phase of baddeleyite exists from ~ 21 – 33 GPa (in helium/neon), or ~ 21 – 50 GPa (methanol-ethanol mixture). Above ~

33 GPa (in helium/neon) or ~ 50 GPa (methanol-ethanol mixture) up to ~ 60 GPa, baddeleyite transforms to TiO_2-OI. The differences in these onset pressures of the baddeleyite → TiO_2-OI transition arise from the differences in the shear moduli of the pressure media after solidification. The non-hydrostaticity of a pressure medium at high pressure makes the baddeleyite → TiO_2-OI transition energetically less favorable than at hydrostatic conditions. This work provides new knowledge of the natural brookite phase transitions at very high pressures (up to ~ 60 GPa), offering insights into how hydrostaticity and the elastic properties of a pressure medium can affect the phase transition behavior under compression. The obtained fundamental understanding of the brookite system may be transferable to other natural mineral systems.

ASSOCIATED CONTENT

Supporting Information

The Supporting Information is available free of charge on the ACS Publications website at DOI:

Effect of non-hydrostaticity on enthalpy, XRD pattern of thin foil brookite, lattice parameters from representative Rietveld fitting,

bulk moduli of TiO_2 phases, shear modulus of methanol at high pressure.

AUTHOR INFORMATION

Corresponding Author

*E-mail: hengzhong.zhang@hpstar.ac.cn, Phone: +86-21-80177095.

ORCID

Hengzhong Zhang: 0000-0003-2322-2274

Notes

The authors declare no competing financial interest.

ACKNOWLEDGMENTS

The high-pressure synchrotron X-ray diffraction was conducted at the high-energy beamline station 12.2.2 of Advanced Light Source, Lawrence Berkeley National Laboratory, Berkeley, California, USA and beamline station 13-BM-C of Advanced Photon Source, Argonne National Laboratory, Argonne, Illinois, USA. Part of the experimental work of this study was conducted at GeoSoilEnviroCARS (Sector 13), Partnership for Extreme Crystallography Program (PX^2), Advanced Photon Source (APS), and Argonne National Laboratory. GeoSoilEnviroCARS is supported by the National Science Foundation-Earth Sciences (EAR-1128799) and Department of Energy-Geosciences (DE-FG02-94ER14466). PX^2 Program is supported by COMPRES under NSF Cooperative Agreement EAR 11-57758. Use of the Advanced Photon Source was supported by the US Department of Energy, Office of Science, Office of Basic Energy Sciences, under Contract No.DE-AC02-06CH11357. We thank Tim Teague (UCB) for providing the natural brookite mineral sample and Yanping Yang (HPSTAR) for assistance in SEM sample characterization.

REFERENCES

(1) Hwang, S. L.; Shen, P.; Chu, H. T. Nanometer-size α-PbO_2-type TiO_2 in garnet: a thermobarometer for ultrahigh-pressure metamorphism. *Science* **2000**, *288*, 321-324.

(2) Dewhurst, J. K.; Lowther, J. E. High-pressure structural phases of titanium dioxide. *Physical Review B* **1996**, *54*, R3673.

(3) Smith, S. J.; Stevens, R.; Liu, S.; Li, G.; Navrotsky, A.; Boerio-Goates, J.; Woodfield, B. F. Heat capacities and thermodynamic functions of TiO_2 anatase and rutile: analysis of phase stability. *American Mineralogist* **2009**, *94*, 236–243.

(4) Zhang, H.; Banfield, J. F. Structural characteristics and mechanical and thermodynamic properties of nanocrystalline TiO_2. *Chemical Reviews* **2014**, *114*, 9613-9644.

(5) Zhang, H.; Banfield, J. F. Understanding polymorphic phase transformation behavior during growth of nanocrystalline aggregates: insights from TiO_2. *The Journal of Physical Chemistry B* **2000**, *104*, 3481-3487.

(6) Zhu, K. R.; Zhang, M. S.; Hong, J. M.; Yin, Z. Size effect on phase transition sequence of TiO_2 nanocrystal. *Materials Science and*

Engineering: A **2005**, *403*, 87-93.

(7) Gribb, A. A.; Banfield, J. F. Particle size effects on transformation kinetics and phase stability in nanocrystalline TiO_2. *American Mineralogist* **1997**, *82*, 717-728.

(8) Howard, J. M. The geology of Arkansas: the natural state. *Rocks & Minerals* **1989**, *64*, 270-276.

(9) Howard, J. M. Brookite, rutile paramorphs after brookite, and rutile twins from Magnet Cove, Arkansas. *Rocks & Minerals* **1999**, *74*, 92-102.

(10) Howard, J. M.; Owens, D. R. Minerals of the Wilson springs vanadium mines: potash sulphur springs, Arkansas. *Rocks & Minerals* **1995**, *70*, 154-170.

(11) Dachille, F.; Simons, P.; Roy, R. Pressure-temperature studies of anatase, brookite, rutile and TiO_2-II. *American Mineralogist* **1968**, *53*, 1929-1939.

(12) Yanqing, Z.; Erwei, S.; Suxian, C.; Wenjun, L.; Xingfang, H. Hydrothermal preparation and characterization of brookite-type TiO_2 nanocrystallites. *Journal of Materials Science Letters* **2000**, *19*, 1445-1448.

(13) Buonsanti, R.; Grillo, V.; Carlino, E.; Giannini, C.; Kipp, T.;

Cingolani, R.; Cozzoli, P. D. Nonhydrolytic synthesis of high-quality anisotropically shaped brookite TiO_2 nanocrystals. *J. Am. Chem. Soc.* **2008**, *130*, 11223-11233.

(14) Lin, H.; Li, L.; Zhao, M.; Huang, X.; Chen, X.; Li, G.; Yu, R. Synthesis of high-quality brookite TiO_2 single-crystalline nanosheets with specific facets exposed: tuning catalysts from inert to highly reactive. *J. Am. Chem. Soc.* **2012**, *134*, 8328-8331.

(15) Xu, Y.; Lin, H.; Li, L.; Huang, X.; Li, G. Precursor-directed synthesis of well-faceted brookite TiO_2 single crystals for efficient photocatalytic performances. *Journal of Materials Chemistry A* **2015**, *3*, 22361-22368.

(16) Jamieson, J. C.; Olinger, B. High-pressure polymorphism of titanium dioxide. *Science* **1968**, *161*, 893-895.

(17) Sato, H.; Endo, S.; Sugiyama, M.; Kikegawa, T.; Shimomura, O.; Kusaba, K. Baddeleyite-type high-pressure phase of TiO_2. *Science* **1991**, *251*, 786-788.

(18) Dubrovinskaia, N. A.; Dubrovinsky, L. S.; Ahuja, R.; Prokopenko, V. B.; Dmitriev, V.; Weber, H. P.; Osorio-Guillen, J.; Johansson, B. Experimental and theoretical identification of a new high-pressure TiO_2 polymorph. *Phys. Rev. Lett.* **2001**, *87*, 275501.

(19) Dubrovinsky, L. S.; Dubrovinskaia, N. A.; Swamy, V.; Muscat, J.;

Harrison, N. M.; Ahuja, R.; Holm, B.; Johansson, B. Materials science: The hardest known oxide. *Nature* **2001**, *410*, 653.

(20) Luo, W.; Yang, S.; Wang, Z.; Wang, Y.; Ahuja, R.; Johansson, B.; Liu, J.; Zou, G. T. Structural phase transitions in brookite-type TiO_2 under high pressure. *Solid State Communications* **2005**, *133*, 49-53.

(21) Clark, S. M.; MacDowell, A. A.; Knight, J.; Kalkan, B.; Yan, J.; Chen, B.; Williams, Q. Beamline 12.2.2: an extreme conditions beamline at the Advanced Light Source. *Synchrotron Radiation News* **2012**, *25*, 10-11.

(22) Kunz, M.; MacDowell, A. A.; Caldwell, W. A.; Cambie, D.; Celestre, R. S.; Domning, E. E.; Duarte, R. M.; Gleason, A. E.; Glossinger, J. M.; Kelez, N. A beamline for high-pressure studies at the Advanced Light Source with a superconducting bending magnet as the source. *J. Synchrotron Rad.* **2005**, *12*, 650-658.

(23) Prescher, C.; Prakapenka, V. B. Dioptas: a program for reduction of two-dimensional X-ray diffraction data and data exploration. *High Pressure Research* **2015**, *35*, 285-288.

(24) Toby, B. H. EXPGUI: a graphical user interface for GSAS. *Journal of applied crystallography* **2001**, *34*, 210-213.

(25) Stutzman, P. E.; Struble, L. *Instructions in Using GSAS Rietveld*

Software for Quantitative X-Ray Diffraction Analysis of Portland Clinker and Cement; NIST TN 1884; National Institute of Standards and Technology, 2015. https://doi.org/10.6028/NIST.TN.1884.

(26) Giannozzi, P.; Andreussi, O.; Brumme, T.; Bunau, O.; Nardelli, M. B.; Calandra, M.; Car, R.; Cavazzoni, C.; Ceresoli, D.; Cococcioni, M. Advanced capabilities for materials modelling with Quantum ESPRESSO. *Journal of Physics: Condensed Matter* **2017**, *29*, 465901.

(27) Nishihara, S. Burai 1.3, A GUI of Quantum ESPRESSO, **2016**. http://nisihara.wixsite.com/burai.

(28) Blöchl, P. E. Projector augmented-wave method. *Physical Review B* **1994**, *50*, 17953.

(29) Perdew, J. P.; Burke, K.; Ernzerhof, M. Generalized gradient approximation made simple. *Physical Review Letters* **1996**, *77*, 3865.

(30) Anisimov, V. I.; Zaanen, J.; Andersen, O. K. Band theory and Mott insulators: Hubbard U instead of Stoner I. *Phys. Rev. B* **1991**, *44*, 943.

(31) Arroyo-de Dompablo, M.; Morales-García, A.; Taravillo, M. DFT + U calculations of crystal lattice, electronic structure, and phase stability under pressure of TiO_2 polymorphs. *The Journal of Chemical Physics* **2011**, *135*, 054503.

(32) Hellenbrandt, M. The inorganic crystal structure database (ICSD)

—present and future. *Crystallography Reviews* **2004**, *10*, 17-22.

(33) Pauling, L.; Sturdivant, J. H. XV. The crystal structure of brookite. *Zeitschrift für Kristallographie - Crystalline Materials* **1928**, *68*, 239-256.

(34) Klotz, S.; Chervin, J.; Munsch, P.; Le Marchand, G. Hydrostatic limits of 11 pressure transmitting media. *Journal of Physics D: Applied Physics* **2009**, *42*, 075413.

(35) Gražulis, S.; Daškevič, A.; Merkys, A.; Chateigner, D.; Lutterotti, L.; Quiros, M.; Serebryanaya, N. R.; Moeck, P.; Downs, R. T.; Le Bail, A. Crystallography Open Database (COD): an open-access collection of crystal structures and platform for world-wide collaboration. *Nucleic Acids Res.* **2012**, *40*, D420-D427.

(36) Desgreniers, S.; Lagarec, K. High-density ZrO_2 and HfO_2: crystalline structures and equations of state. *Physical Review B* **1999**, *59*, 8467.

(37) Adams, D. M.; Leonard, S.; Russell, D. R.; Cernik, R. J. X-ray diffraction study of hafnia under high pressure using synchrotron radiation. *Journal of Physics and Chemistry of Solids* **1991**, *52*, 1181-1186.

(38) Leger, J. M.; Tomaszewski, P.; Atouf, A.; Pereira, A. S. Pressure-

induced structural phase transitions in zirconia under high pressure. *Phys. Rev. B* **1993**, *47*, 14075.

(39) Leger, J. M.; Atouf, A.; Tomaszewski, P.; Pereira, A. S. Pressure-induced phase transitions and volume changes in HfO_2 up to 50 GPa. *Phys. Rev. B* **1993**, *48*, 93.

(40) Tompsett, G.; Bowmaker, G.; Cooney, R.; Metson, J.; Rodgers, K.; Seakins, J. M. The Raman spectrum of brookite, TiO_2 (Pbca, Z= 8). *Journal of Raman Spectroscopy* **1995**, *26*, 57-62.

(41) Iliev, M. N.; Hadjiev, V. G.; Litvinchuk, A. P. Raman and infrared spectra of brookite (TiO_2): experiment and theory. *Vibrational Spectroscopy* **2013**, *64*, 148-152.

(42) Li, Q.; Liu, R.; Liu, B.; Wang, L.; Wang, K.; Li, D.; Zou, B.; Cui, T.; Liu, J.; Chen, Z. Stability and phase transition of nanoporous rutile TiO_2 under high pressure. *RSC Adv.* **2012**, *2*, 9052-9057.

(43) Li, Q. J.; Liu, B. B. High pressure structural phase transitions of TiO_2 nanomaterials. *Chinese Physics B* **2016**, *25*, 076107.

(44) Li, Q.; Liu, R.; Cheng, B.; Wang, L.; Yao, M.; Li, D.; Zou, B.; Cui, T.; Liu, B. B. High pressure behaviors of nanoporous anatase TiO_2. *Materials Research Bulletin* **2012**, *47*, 1396-1399.

(45) Huberty, J.; Xu, H. Kinetics study on phase transformation from

titania polymorph brookite to rutile. *Journal of Solid State Chemistry* **2008**, *181*, 508-514.

(46) Huang, Y.; Chen, F.; Li, X.; Yuan, Y.; Dong, H.; Samanta, S.; Yu, Z.; Rahman, S.; Zhang, J.; Yang, K. Pressure-induced phase transitions of exposed curved surface nano-TiO_2 with high photocatalytic activity. *Journal of Applied Physics* **2016**, *119*, 215903.

(47) Dylla, A. G.; Henkelman, G.; Stevenson, K. J. Lithium insertion in nanostructured TiO_2 (B) architectures. *Chem. Res.* **2013**, *46*, 1104-1112.

(48) Haines, J.; Leger, J.; Schulte, O. The high-pressure phase transition sequence from the rutile-type through to the cotunnite-type structure in. *Journal of Physics: Condensed Matter* **1996**, *8*, 1631.

(49) Lowther, J.; Dewhurst, J.; Leger, J.; Haines, J. Relative stability of ZrO_2 and HfO_2 structural phases. *Phys. Rev. B* **1999**, *60*, 14485.

(50) Mei, Z. G.; Wang, Y.; Shang, S.; Liu, Z. K. First-principles study of the mechanical properties and phase stability of TiO_2. *Computational Materials Science* **2014**, *83*, 114-119.

(51) Nishio-Hamane, D.; Shimizu, A.; Nakahira, R.; Niwa, K.; Sano-Furukawa, A.; Okada, T.; Yagi, T. The stability and equation of state for the cotunnite phase of TiO_2 up to 70 GPa. *Physics and Chemistry of*

Minerals **2010**, *37*, 129-136.

(52) Mei, Z. G.; Wang, Y.; Shang, S. L.; Liu, Z. K. First-principles study of lattice dynamics and thermodynamics of TiO_2 polymorphs. *Inorg. Chem.* **2011**, *50*, 6996-7003.

(53) Fu, Z.; Liang, Y.; Wang, S.; Zhong, Z. Structural phase transition and mechanical properties of TiO_2 under high pressure. *Physica Status Solidi (b)* **2013**, *250*, 2206-2214.

(54) Swamy, V.; Wilson, N. C. First-principles calculations of the pressure stability and elasticity of dense TiO_2 phases using the B3LYP hybrid functional. *J. Phys. Chem. C* **2014**, *118*, 8617-8625.

(55) Liu, Q. J.; Ran, Z.; Liu, F. S.; Liu, Z. T. Phase transitions and mechanical stability of TiO_2 polymorphs under high pressure. *Journal of Alloys and Compounds* **2015**, *631*, 192-201.

(56) Trail, J.; Monserrat, B.; Ríos, P. L.; Maezono, R.; Needs, R. J. Quantum Monte Carlo study of the energetics of the rutile, anatase, brookite, and columbite TiO_2 polymorphs. *Phys. Rev. B* **2017**, *95*, 121108.

(57) Wu, X.; Holbig, E.; Steinle-Neumann, G. Structural stability of TiO_2 at high pressure in density-functional theory based calculations. *Journal of Physics: Condensed Matter* **2010**, *22*, 295501.

(58) Che, X.; Li, L.; Zheng, J.; Li, G.; Shi, Q. Heat capacity and thermodynamic functions of brookite TiO_2. *The Journal of Chemical Thermodynamics* **2016**, *93*, 45–51.

(59) Banfield, J. F.; Veblen, D. R. Conversion of perovskite to anatase and TiO_2(B): a TEM study and the use of fundamental building blocks for understanding relationships among the TiO_2 minerals. *American Mineralogist* **1992**, *77*, 545-557.

(60) Barge, N. V.; Boehler, R. Effect of non-hydrostaticity on the α-ε transition of iron. *High Pressure Research* **1990**, *6*, 133–140.

(61) Grechnev, A.; Tretyak, S. M.; Freiman, Y. A.; Goncharov, A. F.; Gregoryanz, E. Elastic anisotropy and poisson's ratio of solid helium under pressure. *Physical Review B* **2015**, *92*, No.024102.

(62) Zaug, J. M.; Slutsky, L. J.; Brown, J. M. Equilibrium properties and structural relaxation in methanol to 30.4 GPa. *The Journal of Physical Chemistry* **1994**, *98*, 6008–6016.

Graphic for TOC only:

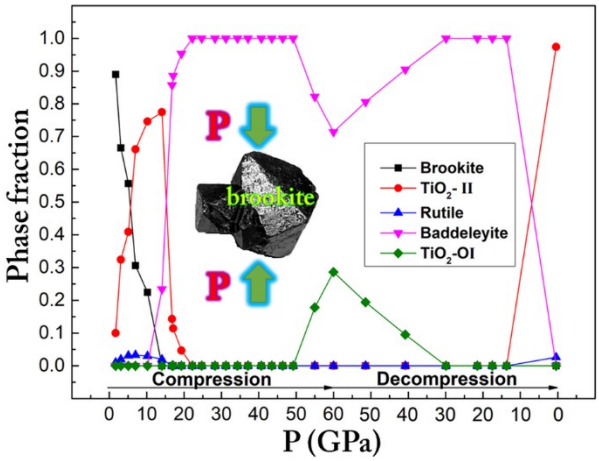
Phase fraction
P (GPa)
Brookite
TiO2- II
Rutile
Baddeleyite
TiO2-OI
P
P
brookite
Compression
Decompression